Diffuse wave spectroscopy for optical properties measurements of normal and coagulated chicken liver using ultrafast femtosecond wavelength range (390-435 nm)

HAFEEZ ULLAH[*], ASIF SHEHZAD, ZAHIDA BATOOL, ALIA NAZIR
Biophotonics Imaging Techniques Laboratory, Department of Physics, The Islamia University of Bahawalpur, Bahawalpur, Pakistan

In this study, we have determined the optical properties (absorption coefficient, scattering coefficient, reduced scattering coefficient and penetration depth of laser radiation) of normal and thermally coagulated chicken liver at wavelengths of 390, 395, 400, 405, 410, 415, 420, 425, 430 and 435 nm of laser irradiation using the Kubelka Munk model from the radial dependence of diffused wave spectroscopy data in the femtosecond short pulsed-laser regime. We have also proved that the diffused signal is not affected by up to 1 minute of data collection from the liver tissue. The absorption and scattering coefficients have been observed to be significantly increased due to the coagulation of the chicken liver at 90 °C. An increasing trend in the calculated values of optical parameters of normal and abnormal chicken liver within 390 nm-435 nm wavelength range has been observed. The total attenuation coefficient has been calculated with the help of absorption and scattering coefficient. We believe that these significant differences in optical properties will be helpful to understand the optimal use of laser application and diagnosis of tissue for different optical therapeutic techniques like photodynamic therapy. This technique can be extended for optical parameter measurements of superficial organs e.g. breast cancer and skin tumors.

1. Introduction

New optical methods for getting information about the tissues, molecules and the treatment of several diseases are the result of progress in technology and science [1]. The information about optical parameters of tissues like scattering coefficient and absorption coefficients plays a vital role in effective applications of lasers in the medical field [2]. Different models, for example, Monte Carlo simulation, Kubelka-Munk model (KMM), inverse Monte Carlo simulation, and integrating sphere measurements [3], sized-fiber reflectometry, Boltzmann transport equation [4], steady state [5, 6], time-resolved [7], inverse adding-doubling (IAD) method, optical coherence tomography (OCT) [8], and oblique incidence optical fiber reflectometry [9] have been described to measure the optical parameters [10-13]. The steady-state diffuse reflectance method is of importance due to its ability to probe changes in the optical properties of individual tissues as well as their relative concentrations [5, 6]. We have implemented KMM for the measurement of optical properties of chicken liver from the diffused wave spectroscopy (DWS) data using femtosecond pulsed laser.

These parameters are extracted from observable quantities including transmission, reflection, and scattering. Among these quantities, scattered light is more suitable for the diagnostic purposes [11]. This *ex-vivo* study represents the measurement of tissue optical properties from diffusely reflected light from the chicken liver to investigate the light distribution in femtosecond short pulse regime. The diffuse reflectance can be defined as the probability of photon reemission per unit surface area from a scattering medium [14]. The significant benefits of DWS include the *in-vivo* and *in-vitro* measurements of human skin, bladder, colon and animal tissues such as rat mucous and brain, etc. On the basis of these results, the DWS provides valuable information and has proved to be a real-time, non-destructive and quantitative means for improving biopsy [15].

DWS is a model of light transport in tissue that relates the values of diffuse reflectance with optical scattering and absorption coefficient of tissues to characterize the bio tissues. Usually, this technique is used by comparing the measured data with optical parameters determined either experimentally or theoretically for the same bio tissue [16]. In radiance within the tissues, the degree of anisotropy can be restricted by diffusion theory. For handling the problem of boundary conditions at the surface of tissues, a particular problem of boundary conditions arises. In order to describe these boundary conditions, various models of changing degrees of sophistication have been developed. For example, in Farrell's work to contact probe instrument a neural network was applied. A reflectance versus the distance curve was used due to

possible changes in optical coupling between the tissues and fibers [17, 18].

For each type of tissue, we have chosen the initial propagation of laser direction as the direction for analysis. We have examined that the behavior of laser light does not depend upon the direction that can be expected from isotropic diffusion. Along with the chosen direction, we have obtained the variation of intensity which is a function of source detector separation (mm). We have plotted a graph between intensity and source-detector separation for normal and abnormal chicken liver separately in the range of wavelength from 390 nm to 435 nm. We have also investigated that diffused intensity is not affected by up to 1 minute of detection time. Using KMM, we have measured successfully *ex vivo* scattering coefficient (μ_s), absorption coefficient (μ_a) and also reduced scattering coefficient ($\mu_s^{'} = \mu_s(1 - g)$ of the aforementioned tissues.

This propagation of light within the tissues is an important issue in the light dosimetry for the case of laser cure. When laser light falls on the tissues and is distributed, it extracts out the information about the tissue's optical properties. Therefore, this work is useful to diagnose the early neoplastic.

2. Materials and methods

2.1. Diffuse wave spectroscopy

The absorption of laser light in the biological tissues due to different intracellular and extracellular ingredients is described by Beer Lambert's law. When laser light falls on the sample, then multiple scatterings happen inside the tissue i.e. caused by cell organelles and macromolecules. So the several mechanisms such as single scatterings and multiple scatterings are involved in the phenomenon. Whereas, multiple scattering is called the diffuse wave spectroscopy (DWS) that extends dynamic light scattering measurements to samples with strong multiple scattering. This multiple scattering also causes the loss of intensity in the presence of absorption. DWS treats the transport of photons through turbid samples as a diffusion process, thereby making it possible to extract the dynamics of scatterers from measured correlation functions. The analysis of DWS data requires knowledge of the path length distribution of photons traveling through the sample. While for flat sample cells this path length distribution can be readily calculated and expressed in analytical form; no such expression is available for asymmetrical sample cells. DWS measurements have therefore typically relied on dedicated setups that use flat sample cells. Here, we show how DWS measurements can be performed in standard dynamic light scattering setups that use chicken liver sample cells. To do so, we have performed simple diffused reflectance measurements from the normal and coagulated chicken liver that yields optical parameters of the tissue using KMM [19].

2.2. Kubelka Munk model (KMM)

When the scattering is dominant over the absorption, KMM is used to separate μ_a and μ_s from diffusely reflected light. In this model, the fraction of the flux lost due to absorption per unit length is denoted by K whereas that for scattering per unit length by S. These parameters are assumed to be uniform throughout the tissue. The reflection from tissue boundaries is not accounted for this model and only diffused light from the tissue in which the index of refraction mismatch exists is used. The mathematical expression for KMM model for the extraction of μ_a and μ_s is [20]:

$$S = \frac{1}{yt} ln \left[\frac{1 - R_d(x - y)}{T_d} \right] \qquad (1)$$

$$\mu_a = \frac{K}{2}, \quad \mu_s = \frac{4S + \mu_a}{3(1 - g)}, \quad K = S(x - 1), \qquad (2a)$$

$$x = \left[\frac{1 - T_d^2 + R_d^2}{2R_d} \right], \quad y = \sqrt{x^2 - 1} \qquad (2b)$$

where t is the thickness of the sample, R_d and T_d are diffused reflectance and transmittances respectively measured experimentally. The anisotropic factor '$g = 0.8$' was used to calculate μ_a and μ_s [5].

2.3. Sample preparation

In this experiment, we purchased the chicken liver from a nearby market for *ex vivo* studies. The liver was boiled for its coagulation in water at 95°C for 5 minutes. When the chicken was slaughtered then the sample was used only within 30–45 minutes. The sample was investigated in its original form. It means we did not divide it into its small pieces. The measured thickness of the sample was nearly 1 cm.

2.4. Methodology

The spectrometer (Avaspec-2048 of Avantes) was used for data acquisition. Single-mode optical fiber was used for data collection from the biological samples at different positions from the point of illumination. The data is collected by dipping the optical fiber into the liver tissue. The optical fiber was moved in the lateral direction from the illumination point with the spatial step of 1 mm and scanned up to 5 mm because after 5 mm the reflected signal was observed to be very weak approximately equal to the noise level of the detection system. The diameter of the fiber dipped into the tissue to collect scattered light was 1 mm whereas the incident beam diameter was also measured to 1 mm with 1 mW of incident laser pulses. At the same time, the transmitted light was measured with the same optical fiber at the same position on the opposite side of the tissue and wavelength, which provided us T_d. Ti:

sapphire laser (Chameleon of Coherent) was used as a femtosecond short-pulse laser source. The laser has a pulse duration of 140 femtosecond (fs) at the peak and 200 fs across the tuning range. Its average power is >2 W and the repetition rate is 80 MHz. The tuning range of the laser was set from 390 nm to 435 nm. The measured intensity for the samples of the normal liver at each wavelength was plotted as a function of the position and Equation (1and 2) was used to determine μ_a and μ_s respectively. A similar procedure of data acquisition and processing was repeated with the coagulated liver. The total attenuation coefficient was calculated with the relation of $\mu_t = \mu_a + \mu_s$. The penetration depth was calculated using $\sqrt{\dfrac{1}{3\mu\left(\mu + \mu\ (1-g)\right)}}$

[4, 21, 22]. The experimental setup is shown in Fig. 1. The power of the laser was reduced by Fresnel reflection using a glass slab. The fiber was dipped each time for the next measurement after 1mm interval.
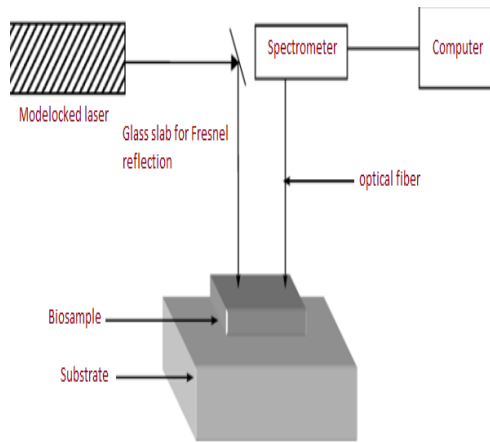

Fig. 1. Experimental setup for the measurement of the optical properties of normal and abnormal chicken liver at wavelength range (390 nm - 435nm)

3. Results

When laser light is incident on the surface of a chicken liver at wavelength range 390 nm to the 435 nm, the light travels inside the tissue to yield out the optical parameters (μ_s, μ_a, μ_s') of the tissue underlying the DWS. The optical fiber was moved to get the M-mode data for temporal measurements. Fig. 2 and Fig. 3 show explicitly that the DWS intensity is approximately constant for the time of ~ 60 Sec for both types of tissues for the wavelength of 390 nm and 410 nm for illustration purpose. The similar behavior has been observed for rest of the wavelengths. Figs 4 and 5 represents the spatial DWS data for both normal and coagulated liver tissue in the ultraviolet regime i.e. 390 nm to 435 nm with the step of 5 nm respectively. The spatial measurements are taken with the step-index of 1 mm up to 5 mm beyond which the data was noise. The behavior of the diffused reflectance data from both normal and coagulated liver is observed to be exponentially decreasing as a function of source-detector separation as predicted earlier. These

measurements yielded the optical parameters μ_a, $\mu_{s,}$ μ_t and penetration depths are given in Tables 1 and 2 for normal and thermally coagulated chicken liver respectively.
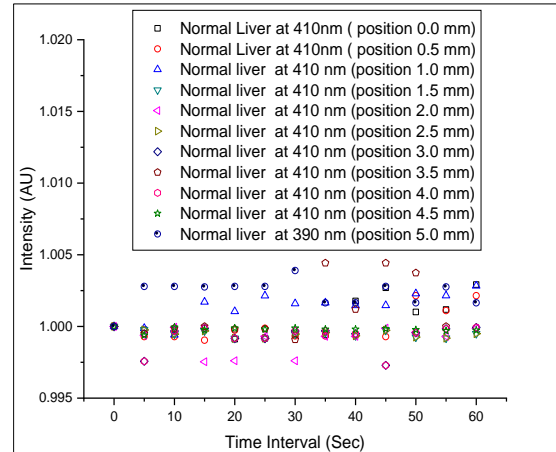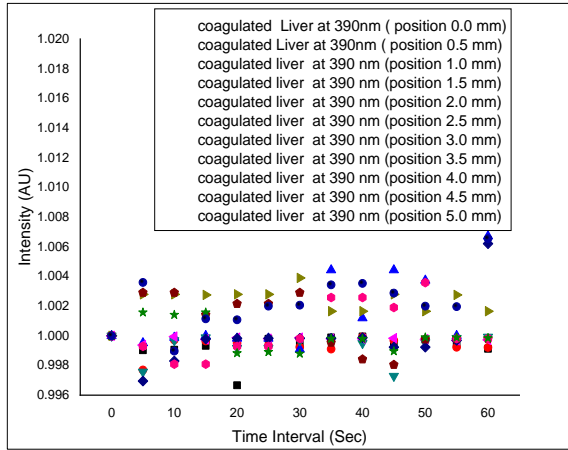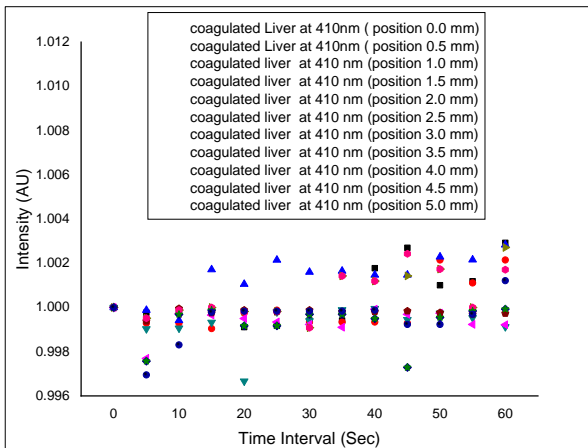

(a)
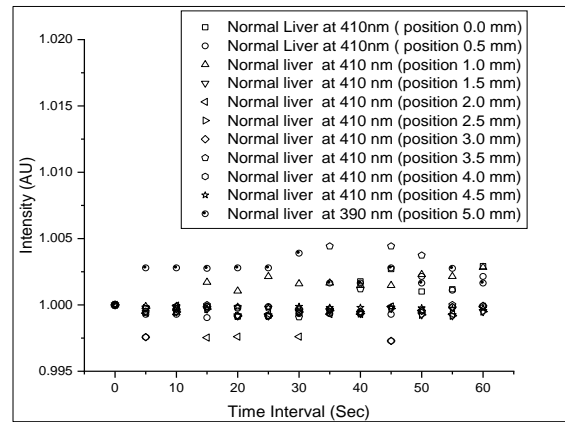
(b)

Fig. 2. Temporal measurements for normal chicken liver at wavelengths of 390 nm, and 410 nm for illustration purpose only. We can see from all the figures that there is no significant change in DWS intensity for 1 minute of the measurements. The same behavior has been observed for rest of the wavelengths (color online)

From Table 1, we can see that the optical properties in normal chicken liver at wavelength range (390 – 435 nm) vary with the wavelength. At wavelength 390 nm, the values of μ_a, μ_s, and μ_s' are 3.065 ± 0.0684, 153.788 and 3.076 cm^{-1} respectively which are different from those values at wavelength 395 nm. As the wavelength increases with the step of 5 nm, the values of optical parameters such as absorption coefficient, scattering coefficient, and reduced scattering coefficient also increase. On the other hand, the optical properties at wavelength range (390 nm – 435 nm) in the thermally coagulated chicken liver also vary significantly. For example, the optical parameters at wavelength 405 nm are different than the values of these optical parameters at other wavelengths. Secondly, the optical parameters for the coagulated liver are different

than the normal liver. The basic reason for this change is that when a chicken liver is thermally heated up to 95 °C, the cell death occurs in the liver.

(a)

(b)

Fig. 3. Temporal measurements for normal chicken liver at wavelengths of 390 nm and 410 nm for illustration purpose only. We can see from all the figures that there is no significant change in intensity for 1 minute of the measurements. The same behavior has been observed for rest of the wavelengths (color online)

According to Terenji *et al* [23], when liver tissues are heated then the optical properties of liver tissues are changed. Hence, it is observed that the scattering is increased at the temperature ranging from 50 to 70 °C. This difference in the aforementioned data may be due to (i) the different size of the particles inside the cells of the liver; (ii) the different type of the animal sources of liver; (iii) the complex structure of the chicken liver and in-homogeneities in the structure of chicken liver; (iv) different environmental conditions during the experiments, (v) the different wavelength and light source used for experiment. However, repeated measurements in our experiments are consistent.

Furthermore, our experiment is in good agreement with the results reported earlier [24] that the scattering intensity of light has exponential decay (Figs. 4 and 5) as

the collecting fiber is translated away from the point of illumination. Optical properties of port wine stain (PWS) skin have been used in PDT experimentations [25].

4. Discussions

Due to coagulation and change in wavelength, there are several reasons for the change of values of μ_a and μ_s. When a cell in the liver tissue is boiled up to a 95 °C, then it cannot be found to remain viable. In this case, cell death can be occurred due to necrosis and apoptosis. The cell killing after coagulation depends upon time and temperature. Therefore, it is impossible for the viability of cells.

In liver tissues, there are many scattering particles which have different refractive indices and sizes. In the liver tissue, small capillaries, cells, collagen fibers, cell nuclei and sub organelles like mitochondria are supposed to be the important centers for the phenomenon of scattering. Whereas, the intracellular and the extracellular fluids behave like a surrounding medium. At the boundaries, where a decrease in the mismatch between surrounding media and scattering centers occurs, the scattering process also decreases. As a result, mismatch in refractive indices in between scattering centers and surrounding media is increased. So the scattering coefficient also increases [26].

After thermal coagulation, the increase in μ_a is due to the denser packing of cells that have the shrinking of the liver. So the number of chromophores cannot change. When a chicken liver is thermally coagulated then due to heat, the hemoglobin is oxidized into methemoglobin. After thermal coagulation at 90 °C in water, the methemoglobin becomes a source of the increase of μ_a. In the arteries of coagulated chicken liver, the collagen blockage would produce the small channels that are called as microchannels. A significant thrombotic occlusion can be produced by the thermal effects. So the increasing temperature tappers the cellular organelles and their fragments like mitochondria, myofilament, and granules inside the mitochondria have decreased because it is a function of temperature from 45 to 75 °C [26]. So a myofilament shows irregular packing at 50 °C and optical properties began to change at 45 °C [27].

The thermal coagulation of the liver is the fragmentation of the liver constituents that can be achieved by laser ablation as well. Pahk *et al.* [28] have investigated the liver tissue exposed to different high intensity focused ultrasound (HIFU) fields (thermal ablation and boiling histotripsy exposure cases). Examining the thermal ablation and the boiling histotripsy exposures, it has been observed that higher-order multiple harmonics, as well as higher levels of broadband emissions, occurred during the boiling histotripsy insonation. These features can, therefore, be used to monitor (a) the different types of cavitation activity for either a thermally or a mechanically induced lesion and (b) the onset of a boiling bubble at the HIFU focus in the course of HIFU exposure. The numerical approach described in this work can be used for predicting cavitation activity under a given HIFU exposure condition.
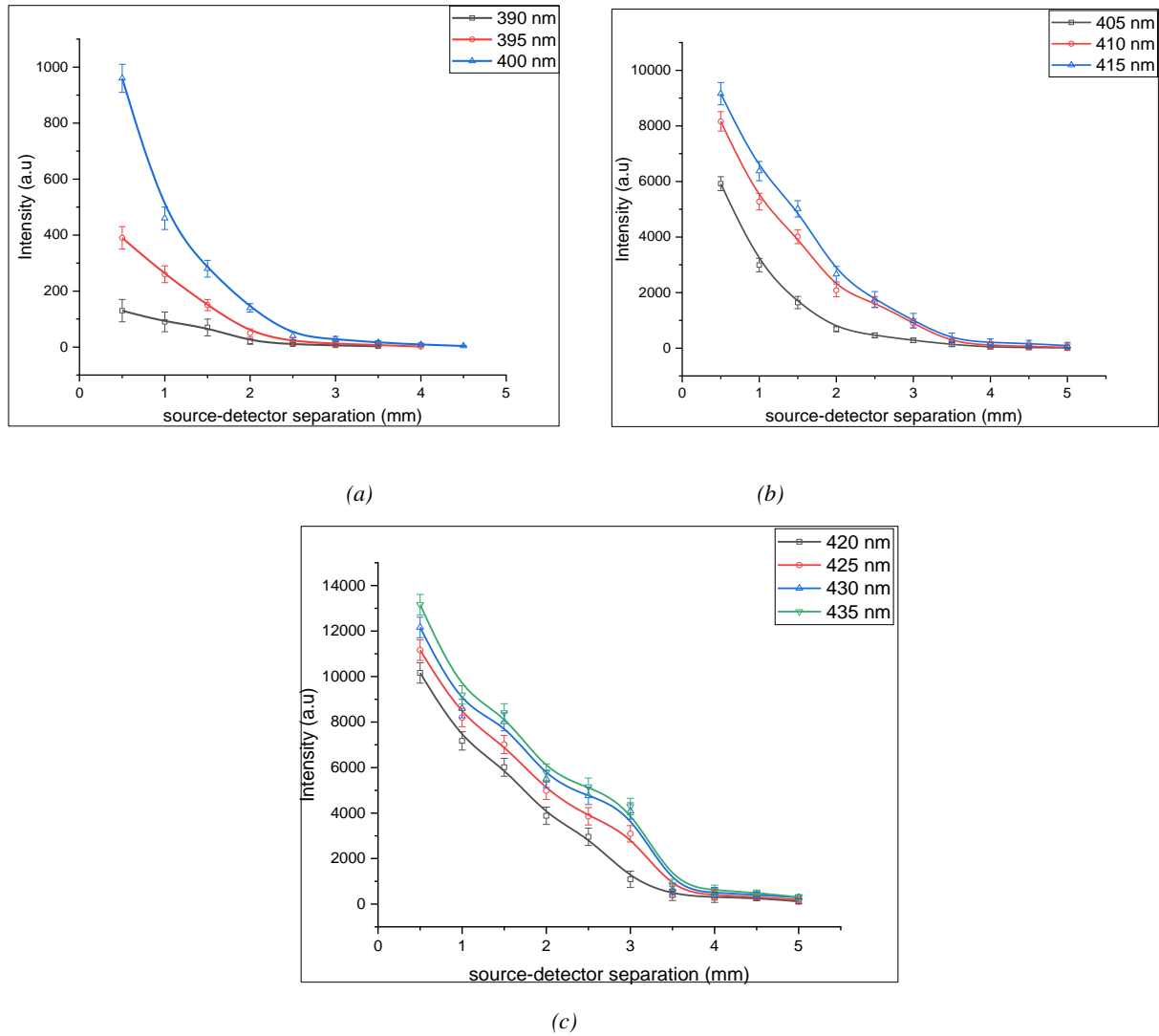
(a)

(b)

(c)

Fig. 4. Diffuse wave spectroscopy intensity for normal Chicken liver at wavelength range (a) (390-400 nm), (b) (405-415 nm), and (c) (420-435 nm). The figure shows the normal exponential behavior of the DWS intensity (color online)

Table 1. Optical properties (absorption and scattering coefficient, penetration depth) in normal chicken liver at wavelength range (390-435 nm)

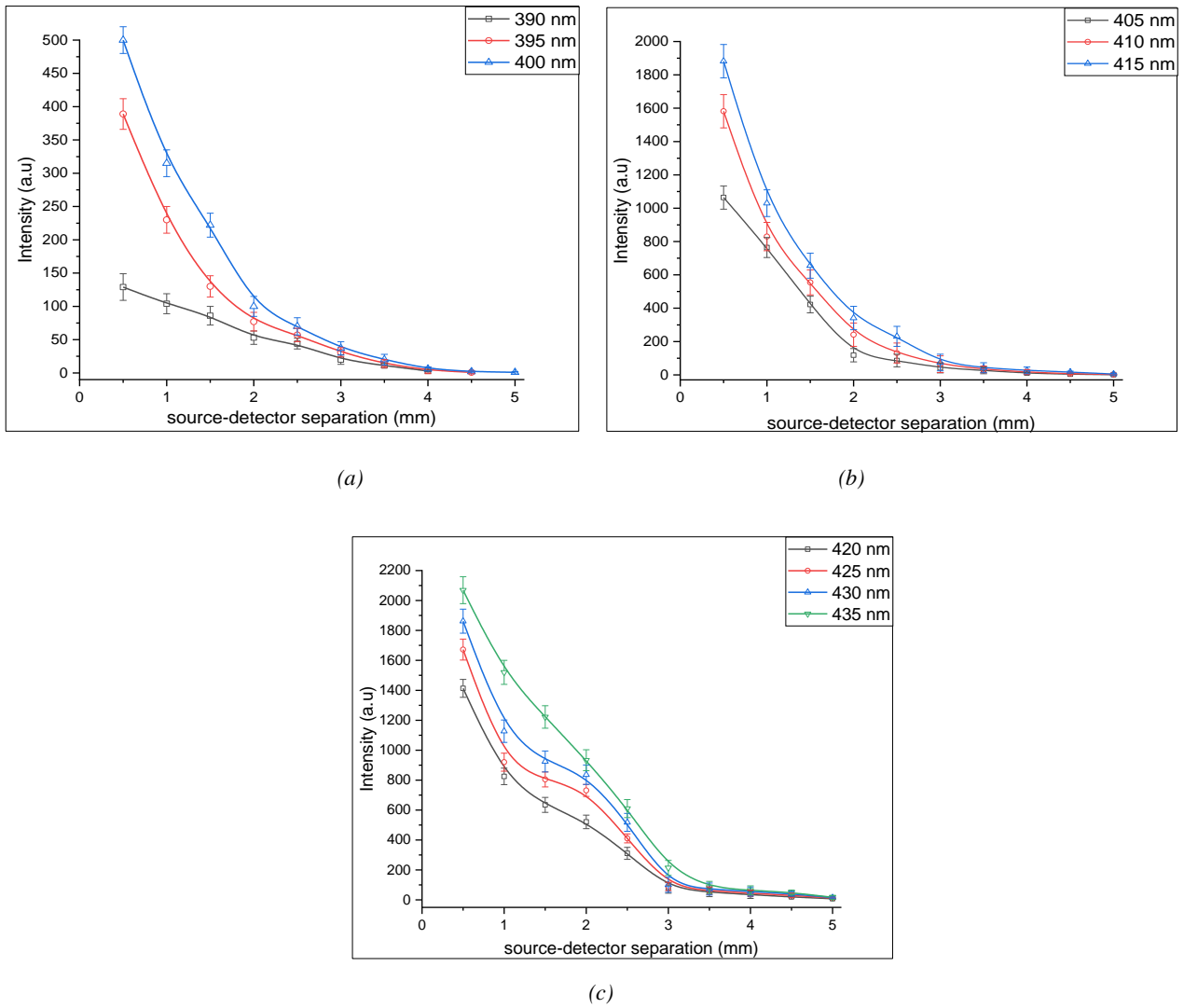| Wavelength (nm)	Absorption Coefficients μ_a (cm^{-1})	Scattering Coefficients μ_s (cm^{-1})	Total attenuation Coefficients (cm^{-1}) μ_t	Reduced scattering Coefficients $\mu_s^{/}$ (cm^{-1})	Penetration Depth (cm) x10^{-3}
390	3.065 ± 0.068	153.785 ±3.579	156.850 ±3.653	3.076 ± 0.068	13.308
395	3.143 ± 0.041	157.621 ±2.482	160.764 ±2.533	3.152 ± 0.041	12.978
400	3.198 ± 0.026	160.259 ±1.857	163.457 ±1.896	3.205 ± 0.026	12.760
405	3.201 ± 0.037	160.429 ±1.630	163.629 ±1.664	3.208 ± 0.031	12.749
410	3.243 ± 0.052	162.607 ±1.111	165.850 ±1.134	3.252 ± 0.068	12.579
415	3.251 ± 0.057	162.828 ±1.055	166.078 ±1.076	3.257 ± 0.068	12.553
420	3.263 ± 0.031	163.424 ±0.931	166.687 ±0.950	3.269 ± 0.044	12.506
425	3.271 ± 0.017	163.791 ±0.854	167.062 ±0.872	3.276 ± 0.030	12.476
430	3.289 ± 0.012	164.678 ±0.581	167.967 ±0.593	3.293 ± 0.029	12.408
435	3.306 ± 0.016	165.500 ±2.279	168.806 ±1.356	3.310 ± 0.022	12.345

(a)

(b)

(c)

Fig. 5. Diffuse wave spectroscopy intensity for coagulated chicken liver at wavelength range (a) (390-400 nm), (b) (405-415 nm), and (c) (420-435 nm). The figure shows the normal exponential behavior of the DWS intensity (color online)

Table 2. Optical properties (absorption and scattering coefficient, penetration depth) in thermally coagulated chicken liver at wavelength range (390-435nm)

Wavelength (nm)	Absorption Coefficients μ_a (cm^{-1})	Scattering Coefficients μ_s (cm^{-1})	Total attenuation Coefficients (cm^{-1}) μ_t	Reduced scattering Coefficients $\mu_s^{/}$ (cm^{-1})	Penetration Depth (cm) x10^{-3}
390	4.069 ± 0.886	203.557 ± 7.035	207.626 ± 7.191	4.071 ± 0.698	10.031
395	4.083 ± 1.001	204.206 ± 6.594	208.288 ± 6.740	4.084 ± 0.789	9.998
400	4.158 ± 1.173	207.927 ± 5.862	212.079 ± 5.990	4.158 ± 0.929	9.819
405	4.191 ± 1.077	209.696 ± 5.450	213.987 ± 5.602	4.194 ± 0.156	9.739
410	4.207 ± 0.886	210.506 ± 5.106	214.713 ± 5.227	4.211 ± 0.698	9.703
415	4.223 ± 0.818	211.270 ± 4.321	216.311 ± 4.423	4.225 ± 0.646	9.667
420	4.388 ± 0.847	219.582 ± 1.419	224.817 ± 1.447	4.392 ± 0.677	9.302
425	4.387 ± 0.871	219.540 ± 1.554	224.799 ± 1.585	4.391 ± 0.701	9.303
430	4.406 ± 0.891	220.445 ± 1.501	225.741 ± 1.530	4.410 ± 0.720	9.265
435	4.448 ± 0.102	222.568 ± 1.035	227.118 ± 7.191	4.451 ± 0.102	9.177

Vogl *et al.* [29] have reported the radiofrequency (RF) ablation, microwave (MW) ablation and laser-induced thermotherapy (LITT) in terms of local progression, survival indexes and major complications in patients with colorectal cancer liver metastases (CRLM) when resectable. Recently, local or regional therapies such as thermal ablations have been used with acceptable outcomes. The median survival in these methods was 33.2, 29.5 and 33.7 months, respectively. Laser-induced thermotherapy may be an appropriate alternative in patients with CRLM who have inoperable liver lesions or have operable lesions as an adjunct to resection.

For each type of tissue, we have chosen the initial propagation of laser light as the direction for analysis. We have examined that the behavior of laser light does not depend upon the direction that can be expected from isotropic diffusion. Along with the chosen direction, we have obtained the variation of intensity which is a function of source-detector separation (mm). So, we have plotted a graph (Figs. 4 and 5) between intensity (au) and source-detector separation (mm) for normal and thermally coagulated chicken liver separately for trend verification as well as for intensity measurements. We observe that as wavelength is increased, the remission of light intensity is also increased. This phenomenon is due to the nature of scattering. We have significantly verified that DWS intensity is constant up to 1 minute for both normal and coagulated liver. This behavior is shown in Fig. 3 (a and b) for both types of tissues respectively.

The collagen blockage in the arteries of the coagulated liver tissue would result in small channels that can be called micro-channels in the lesions and these channels may either remain within the artery or exit through it would cause increased scattering. The arterial plaques are prone to rupture the arteries and lipid in the blood whose size and refractive indices change with temperature can be assumed the strongest scatterers in the coagulated tissue. Also, the thermal effects can induce a significant thrombotic occlusion and can be proved that gradually increasing temperature tapers the cellular organelle [30].

In summary, we have analyzed the impacts of coagulation on the optical parameters of the chicken liver. Using KMM, the absorption and scattering coefficients along with penetration depth were examined in chicken liver. At these five different wavelengths, there are significant differences in values of optical parameters in normal as well as thermally coagulated chicken liver. Due to coagulation, these optical properties can be increased. Also, large differences in optical properties are suggested to be due to large differences in structure and composition between both normal and thermally coagulated chicken liver.

5. Conclusions

In this study, we have investigated a femtosecond pulsed laser light that falls on the chicken liver at five different wavelengths in the range from 309 nm-410 nm. The absorption (μ_a), scattering (μ_s), reduced scattering coefficients (μ_s') and penetration depths were determined using the Kubelka Munk model for both normal and coagulated chicken liver. The differences in measured optical parameters reflect that both the normal and thermally coagulated chicken liver tissues in its composition and structure are different. We observe the reduced penetration depth for the coagulated chicken liver as compared to normal chicken liver encountered with femtosecond pulsed laser. This method can be used for organs e.g skin tumors, breast cancer, rat liver and skin and epithelial tissues at various wavelength ranges. It is observed that the optical parameters measured from the experiment have a smaller difference at each wavelength. These optical parameters carry very useful information for clinical application such as the treatment of cancer such as photodynamic therapy (PDT). We have observed exclusively that, in the wavelength range of 390 nm–435 nm, the absorption coefficient, and scattering coefficient were increased and penetration depth was decreased. When chicken liver tissue is thermally coagulated, scattering process was activated. So the scattering coefficient is increased by the scattering of light energy with tissues. In this way, it is difficult for a light propagation into a deeper area. Hence, DWS with the use of an optical probe is a powerful tool to quantify the optical properties of tissues.

References

[1] J. Mobley, T. Vo-Dinh, Biomedical Photonics Handbook: Fundamentals, Devices, and Techniques, CRC Press, Taylor & Francis group, USA, Chapter No.2, 4 (2014).

[2] H. Ullah, E. Ahmed, M. Ikram, Laser Physics **24**(2), 025601 (2014).

[3] J. W. Pickering, S. A. Prahl, N. van Wieringen, J. F. Beek, H. J. C. M. Sterenborg, M. J. C. van Gemert, Applied Optics **32**(4), 399 (1993).

[4] N. Dögnitz, G. Wagnières, Lasers in Medical Science **13**(1), 55 (1998).

[5] A. Kienle, L. Lilge, M. S. Patterson, R. Hibst, R. Steiner, B. C. Wilson, Applied Optics **35**(13), 2304 (1996).

[6] M. G. Nichols, E. L. Hull, T. H. Foster, Applied Optics **36**(1), 93 (1997).

[7] M. S. Patterson, B. Chance, B. C. Wilson, Applied Optics **28**(12), 2331 (1989).

[8] M. S. Patterson, J. D. Moulton, B. C. Wilson, K. W. Berndt, J. R. Lakowicz, Applied Optics **30**(31), 4474 (1991).

[9] S.-P. Lin, L. Wang, S. L. Jacques, F. K. Tittel, Applied Optics **36**(1), 136 (1997).

[10] C.-L. Tsai, Y.-F. Yang, C.-C. Han, J.-H. Hsieh, M. Chang, Applied Optics **40**(31), 5770 (2001).

[11] W. F. Cheong, S. A. Prahl, A. J. Welch, IEEE Journal of Quantum Electronics **26**(12), 2166 (1990).

[12] V. T. Valerii, Physics-Uspekhi **40**(5), 495 (1997).

[13] H. Ullah, M. Atif, S. Firdous, M. S. Mehmood, M. Y. Hamza, M. Imran, G. Husain, M. Ikram, Optics and Spectroscopy, **110**(2), 313-319 (2010).

[14] L. V. Wang, H. I. Wu, Biomedical Optics (Principles and Imaging), John , Wiley & Sons, Hobokon, New Jersy, USA, 106(2007).

[15] L. Zhang, Journal of Modern Optics **56**(5), 632 (2009).

[16] H. Ullah, M. Atif, S. Firdous, M. S. Mehmood, M. Ikram, C. Kurachi, C. Grecco, G. Nicolodelli, V. S. Bagnato, Laser Physics Letters **7**(12), 889 (2010).

[17] T. J. Farrell, B. C. Wilson, M. S. Patterson, Physics in Medicine & Biology **37**(12), 2281 (1992).

[18] E. H. Derek, J. F. Thomas, S. P. Michael, C. W. Brian, Physics in Medicine & Biology **46**(2), 369 (2001).

[19] Z. Fahimi, F. J. Aangenendt, P. Voudouris, J. Mattsson, H. M. Wyss, Physical Review E **96**(6), 062611 (2017).

[20] V. V. Tuchin, Tissue Optics: Light Scattering Methods and Instruments for Medical Diagnosis, SPIE Press, USA, Second Edition, Vol. PM166, 193(2007).

[21] P. N. Prasad, Introduction to Biophotonics, John Wiley & Sons, USA, 171(2004).

[22] M. H. Niemz, Laser-Tissue Interactions: Fundamentals and Applications, Springer Berlin Heidelberg, Germany, 37(2013).

[23] S. O. Konorov, L. A. Mel'nikov, A. A. Ivanov, M. V. Alfimov, A. V. Shcherbakov, A. M. Zheltikov, Laser Physics Letters **2**(7), 366 (2005).

[24] J. Ferreira, C. K., C. A. S. Melo, L. T. Moriyama, S. Zucoloto, V. S. Bagnato, Laser Physics **14**(2), 209 (2004).

[25] Y. Wang, Z. Zuo, Y. Gu, N. Huang, R. Chen, B. Li, H. Qiu, J. Zeng, J. Zhu, J. Liang, Journal of Biomedical Optics **17**(6), 068003 (2012).

[26] A. Huilan, X. Da, W. Huajiang, G. Huaimin, W. Guoyong, L. Jianjun, Physics in Medicine & Biology **53**(8), 2197 (2008).

[27] S. Bosman, Applied Optics **32**(4), 461 (1993).

[28] K. J. Pahk, P. Gélat, H. Kim, N. Saffari, Ultrasound in Medicine & Biology **44**(12), 2673 (2018).

[29] T. J. Vogl, P. Farshid, N. N. N. Naguib, A. Darvishi, B. Bazrafshan, E. Mbalisike, T. Burkhard, S. Zangos, La radiologia medica **119**(7), 451 (2014).

[30] N. R. Munce, G. A. Wright, A. Mariampillai, B. A. Standish, M. K. K. Leung, L. Tan, K. Lee, B. K. Courtney, A. A. Teitelbaum, B. H. Strauss, I. A. Vitkin, and V. X. D. Yang, J. Biomed. Opt. **15**(1), 011103 (2010).

_____

*Corresponding author: hafeezullah@iub.edu.pk